

Purdue University

Purdue e-Pubs

International Compressor Engineering
Conference

School of Mechanical Engineering

2022

Modeling a Spool Compressor Using a Coupled Fluid And Solid Solver With Cut-Cell Based CFD Methodology With Adaptive Mesh Refinement

Ameya Waikar

David Rowinski

Greg Kemp

Joe Orosz

Craig Bradshaw

Follow this and additional works at: <https://docs.lib.purdue.edu/icec>

Waikar, Ameya; Rowinski, David; Kemp, Greg; Orosz, Joe; and Bradshaw, Craig, "Modeling a Spool Compressor Using a Coupled Fluid And Solid Solver With Cut-Cell Based CFD Methodology With Adaptive Mesh Refinement" (2022). *International Compressor Engineering Conference*. Paper 2716.
<https://docs.lib.purdue.edu/icec/2716>

This document has been made available through Purdue e-Pubs, a service of the Purdue University Libraries.
Please contact epubs@purdue.edu for additional information.
Complete proceedings may be acquired in print and on CD-ROM directly from the Ray W. Herrick Laboratories at
<https://engineering.purdue.edu/Herrick/Events/orderlit.html>

Modeling a Spool Compressor Using a Coupled Fluid And Solid Solver With Cut-Cell Based CFD Methodology With Adaptive Mesh Refinement

Ameya WAIKAR^{1*}, David ROWINSKI¹, Greg KEMP², Joe OROSZ², Craig BRADSHAW³

¹Convergent Science, Inc.
Madison, WI, USA
608-230-1596, ameya.waikar@convergecf.com
david.rowinski@convergecf.com

²Torad Engineering LLC
Alpharetta, Georgia, USA
greg.kemp@toradengineering.com
joe.orosz@toradengineering.com

³Oklahoma State University, Stillwater, OK USA
craig.bradshaw@okstate.edu

* Corresponding Author

ABSTRACT

The novel spool compressor provides a new rotating compression mechanism with applications in residential and commercial air conditioning systems. The spool compressor features a rotor and a constrained sliding vane which create a positive-displacement compression process. An array of poppet valves allows for the discharge of the compressed fluid. The combination of the suction process, the compression process, and the discharge process exhibit a strong degree of interdependence on the fluid flow and the motion of the components. It is essential to understand this complex fluid flow and its interaction with the moving components inside the compressor to improve its design and efficiency. Computational Fluid Dynamics (CFD) has been increasingly used for the design and analysis of compressors. The spool compressor's interconnected components undergo both translation and rotation, and the valve motion is dependent on the flow field. These factors make the process of defining the computational grid on which the governing equations are solved highly non-trivial. Furthermore, in these models, it is imperative to ensure the grid discretization yields a sufficiently small numerical error relative to the experimental, modeling, and gross error.

This paper deals with the development and application of a CFD model for a spool compressor. An automatic meshing approach is used to tackle the challenge of moving geometries. Furthermore, adaptive mesh refinement is used to dynamically change the mesh based on local velocity and temperature at each time step. Thus, the Cartesian cut-cell based meshing requires no user meshing, with the mesh concentrated in the regions of large gradients. An explicit coupled approach is used to account for the fluid-structure interaction between valves and the flow field. The displacement of each of the valves is constrained in one dimension along the valve post. The fluid is solved using a finite volume approach, whereas equations of rigid body motion are used to solve for the valve motion of an arbitrary number of discharge valves. The working fluid used for the simulation is R134a. Experimental data for mass flow rate, torque, and pressure traces at various locations is used to validate the CFD model. The results from the simulation show good agreement for the global quantities of mass flow rate and power for nearly all mesh sizes, while the instantaneous pressure traces show more sensitivity to the grid size. An appropriately fine interior mesh can resolve the internal pressure fluctuations. Furthermore, the three-dimensional flow field provides insight into valve lifts and flow across the vane tip, as well as the process efficiency.

1. INTRODUCTION

The working of the rotating spool compressor was first described in Kemp et al. (2008). In order to optimize the compressor design for high volumetric efficiency and low power consumption, it is essential to understand the complex fluid flow inside the compressor. It is also important to study the effects of changes in the vane motion and valve placement on the efficiency of the compressor. Bradshaw et al. (2012 and 2016) provide a comprehensive compressor model for estimating the volumetric efficiency and power consumption as a function of various geometric parameters, vane motion, refrigerant properties, and loss in the slip paths. The model predicts the efficiency within a reasonable margin of error for limited operating conditions. However, this model doesn't provide insight into detailed flow physics inside the compressor and doesn't incorporate detailed valve modeling, limiting the ability of the one-dimensional model to capture those variations across a wide range of compressor displacements and operating conditions.

The 3D CFD simulation coupled with fluid-structure interaction (FSI) has shown to provide better accuracy compared to simplified models, especially for cases with complicated and moving geometries. Examples of similar applications of this method in modeling positive displacement compressors include the reed-valve refrigeration reciprocating compressors in Rowinski and Davis (2016) and Rowinski et al. (2018), as well as reed-valve refrigeration scroll compressors in Pham et al. (2018) and reed-valve refrigeration rolling piston compressors in Zhang et al. (2019). These works have shown the method used in this study as an accurate method for computing overall mass flow rate, power consumption, and local pressure traces compared to validated experimental data. In this study, a similar method is applied to a spool compressor, where the main differences are the range of operating conditions and working fluids, the motion of the spool and rotor, and the type of valves used to govern the discharge process.

This study provides a new CFD approach based on the cut-cell method for the spool compressor. The cut-cell based model allows general arbitrary motion without compromising on mass, momentum, and energy conservation. This is particularly helpful for simulating the motion of the vanes and valves. Adaptive Mesh Refinement (AMR) is used to dynamically allocate cells at locations with high gradients. Finally, the results from this study are compared with the provided measured data for three different operating conditions. Mass flow rate, power consumption, and indicator diagrams are the variables of interest. Four different grid sizes are also compared for one of the operating conditions to show grid convergence.

2. CASE SETUP AND DESCRIPTION

The CAD assembly for the compressor was used to construct an enclosed path for the working fluid and exported into a triangulated surface format. The swept volume for this compressor is 801 cubic centimeters. The next sections describe the geometry and operating conditions in more detail.

2.1 Geometry and operating conditions

Figure 1 depicts the details of the construction of the compressor (A), the array of valves connecting the compression and discharge region (B), and the rotor (C6) and vanes (C7) in the compressor region (C). The gas flow path begins at the suction inlet (A1) and goes into the compressor region through the suction manifold. The compressor region is divided into three chambers: suction, compression, and discharge chambers. The chambers are demarcated by the top dead center (TDC) and the tip seals. The eccentricity between the rotor and housing causes the volumes of these chambers to change with time which compresses the gas and then moves to the discharge region through the valves. The compressor contains nine valves (B5), which are divided into three sets of valves for purpose of naming. Each valve has a number and letter assigned to it, the numbering goes from one to three from (left to right), while the letters A-D are assigned based on the column (from top to bottom) for rows one and two, the single valve in row three only has the letter "3" assigned to it. The examples of this naming convention are shown in red text in (B). The gas then moves from the discharge region into the motor cavity region (A4). The gas exits the domain through the outlet at the bottom. The compressor is designed to work for various refrigerants but this study focuses on R134a as the working fluid. Table 1 shows the operating conditions that are tested in this study, one high load, one medium load, and one low load condition

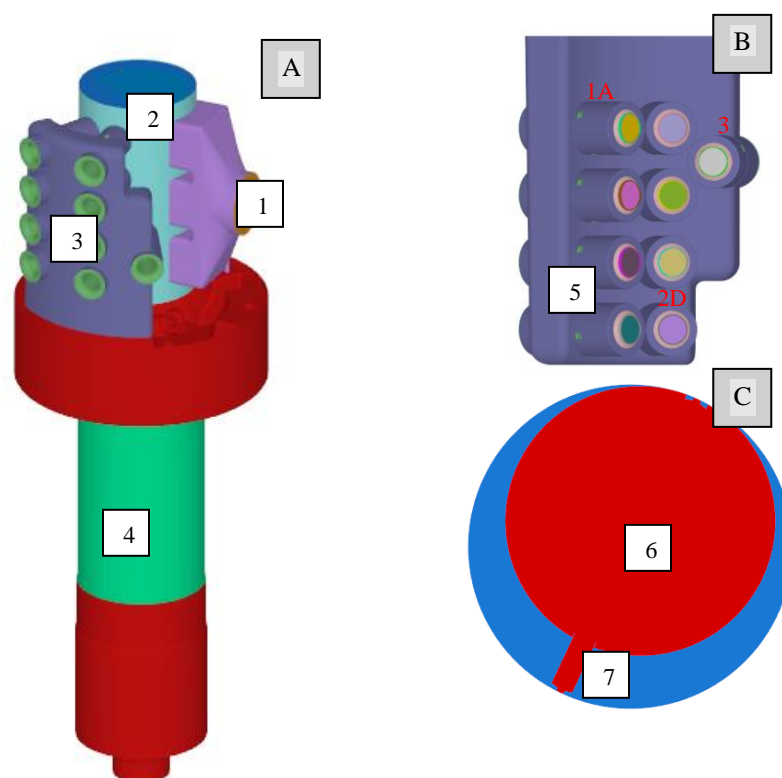


Figure 1: (A) shows the entire computational domain, (B) shows the array of valves between the compression and discharge region and (C) shows the vanes and rotor.

Case Name	Inlet Pressure [MPa]	Outlet Pressure [MPa]	Rotor Speed [RPM]
Case 21	0.34	1.47	1730
Case 26	0.34	1.28	1740
Case 30	0.34	0.96	1760

Table 1: Operating pressures and RPM studied in this study.

2.2 Measurements

It is essential to measure the pressure and volume as a function of time to construct a pressure-volume curve. The details of the experimental measurements are described in Yarborough *et al.* (2021). The Meggitt 8530B-500 high-speed pressure sensors are used at five different locations. As seen in Figure 2 (A), three sensors are located in the compression region, namely: suction sensor (SP), compressor sensor (PP), and discharge sensor (DP), they are located at 90 degrees, 249 degrees, and 343 degrees from the TDC respectively. The measurements from these three sensors are used to construct the pressure-volume curve for the compressor. Additionally, two more pressure sensors are placed on the discharge plenum (DP) and motor cavity (MC), which are highlighted in Figure 2 (B). The pressure sensors are sampled at 70,000 samples per second for 20 times per operating condition. A hall-effect proximity sensor is also installed to measure the shaft rotational angle. An analytical formula is then used to calculate volume from the shaft rotational angle. The shaft power is calculated from the input power measured by a wattmeter and using the motor efficiency, which is known. A variable frequency drive (VFD) is used to control the motor frequency and fix the RPM for the rest conditions. Yarborough *et al.* (2021) provides 36 test conditions out of

which three are chosen for comparison in this study. The maximum propagated error in this study was shown to be 0.85%

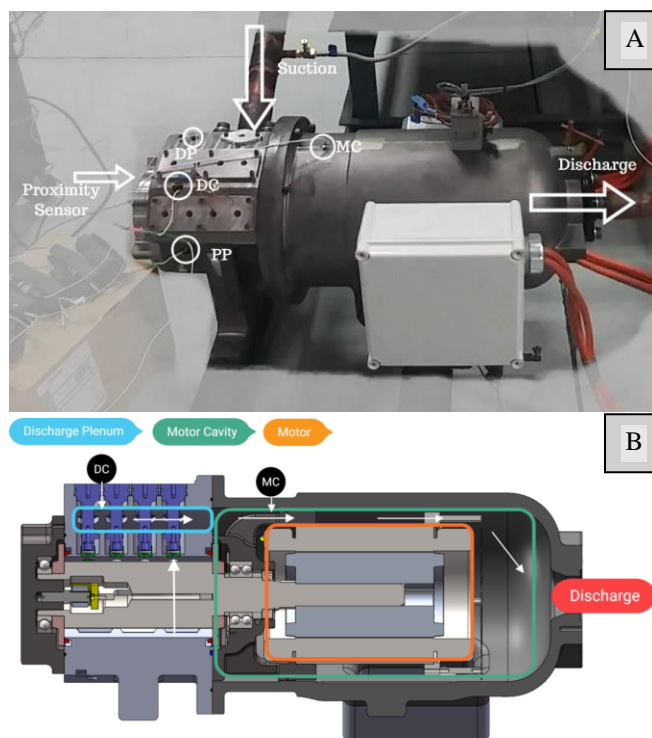


Figure 2: (A) shows the experimental setup used to obtain the measurements, (B) shows a section view of the CAD model

3. METHODOLOGY

The numerical method used in this study is similar to that in Pham *et al.* (2018) and Rowinski *et al.* (2018a, 2018b). The mesh is generated at run time using a cut-cell based approach as described by Senecal *et al.* (2007). The volume is filled with orthogonal cartesian cells controlled by a user-specified base grid size. The triangulated surface is used to cut cells into arbitrarily sized polyhedra at the boundaries of the fluid domain. The cut-cells are formed at every time step at the moving boundaries. This feature helps to handle arbitrary shaped boundaries and complex boundary motion. AMR, as described in Pomraning *et al.* (2014), adds additional cells based on gradients of the specified flow variables.

3.1 Flow Solver

The finite-volume method is used to solve the conservation equations for mass, momentum, energy, and turbulence quantities at the cell centers. To avoid the checker-boarding in the pressure and velocity fields, the algorithm by Rhie and Chow (1983) is used. The pressure implicit with splitting of operators (PISO) method of Issa (1985) is used for pressure-velocity coupling. A second-order central scheme is used for discretization in space and a first-order fully implicit scheme is used to discretize in time. Momentum, density, energy, and turbulence variables are solved using the successive over-relaxation (SOR) iterative method, while high-performance preconditioners (HYPRE) biconjugate gradient stabilized (BiCGSTAB) solver is used to solve for the pressure field. The Re-Normalized Group (RNG) k-epsilon as described by Yakhot (1986) is used for modeling turbulence. Courant-Friedrichs-Lewy (CFL) numbers based on cell size, velocity speed of sound, and diffusivity are used to control the time-step and maintain stability. The thermodynamic and transport properties are computed from structured lookup tables using the software libraries as described in Bell (2014) and the properties from Tillner-Roth and Baehr (1994), which provide more accurate values than other equations of state.

3.2 Fluid – Solid Coupling

The valve motion is an essential part of the simulation and is easy to incorporate using the cut-cell method. The valves are treated as point mass objects located at the center of mass of the object. Fluid forces on the valves are calculated by integrating the stress tensor over the area exposed to the fluid for the viscous force and computing the pressure forces on the projected area in each direction. Spring constants and pre loads are provided as inputs, and the displacement and pre load are used to calculate the spring force on the valve. The fluid and spring forces along with other external forces (ex. gravity) are incorporated into the left-hand side of equation (1) of motion to solve for the displacement. The valves are constrained to move only in one direction along the valve posts, and at the limiter, a coefficient of restitution of zero is applied.

$$F_{total} = m \ddot{x} \quad (1)$$

3.3 Sealing and Gap Flow Modeling

The compressor exhibits several key geometrical areas of small gaps, and how these are treated by the CFD model may have a large impact on the calculated performance. The key gap areas include the axial gap between the rotor and sliding vane to the housing, the radial gap between the rotor and housing, the radial gap between the vane tip and the housing, the gaps between the valve guides and the valve posts, and the gaps between the valves and the valves seats. Depending on several features, including the geometric complexity, the relative importance of the gap on the device efficiency, and the geometric certainty or uncertainty in the actual gap size, a variety of approaches may be used to handle each gap type in the computational model.

The gap between the axial faces of the rotor and vanes and the housing is very small relative to the rotor length and a mechanical seal may be used here, hence the slip flow through this gap can be ignored. A numerical sealing method is applied to these axial faces to cut off the flow in this direction. The seals use projections from the rotor and vanes onto the housing axial faces to identify the slip flow regions at every time step, and surface triangulation is re-computed at every time step. This helps to run the simulation more stably and faster. At the gaps between the valve seats and the valve faces, a slightly similar technique is used, however, a parameter is used to determine when the valve should be opened to the flow and when it should be considered fully sealed. In this model, that value is chosen to be 1 micron, a number very small relative to the overall travel of the valve.

At the radial gaps, both between the vane tips and the housing and between the rotor and the housing, a different technique is applied. Due to geometric uncertainty as well as instantaneous local displacement due to thermal and mechanical loads, it may be difficult to quantify the gap size precisely. Furthermore, with the applied cut-cell based grid resolution technique, it is computationally expensive to attempt to fully resolve the flow in the gaps. Based on these factors, a technique similar to that in Rowinski et al. (2018c), Rowinski et al. (2018c), and Zhang et al. (2019) where a similar problem occurred in the modeling of screw compressors, screw expanders, and rolling piston compressors, respectively. As described in Rowinski et al. (2018c), the method applies a computationally efficient approach in which the gap flows are modeled instead of fully resolved. This is accomplished by applying a momentum sink which acts to account for the effect of unresolved viscosity on a relatively coarse grid. The model term for the amount of the momentum sink is determined through calibration of fully resolving the gap flow on a simpler geometry and then applying a porous media on a coarser grid so that the coarser grid recovers the mass flow rate through the gap as the finer fully resolved grids. In this way, the details of the gap flow boundary layer are not predicted in the coarser model, however, the solution is a very computationally feasible approach when the main simulation objectives are the flow characteristics of the internal compression, suction, and discharge processes. As shown in Rowinski et al. (2019), this method performed compared to measured data for screw expanders at various gap sizes between 80-240 microns.

4. RESULTS AND DISCUSSION

The inlet mass flow rate and average pressure in the compression region are monitored cycle-over-cycle to compute the steady state. The quantities are periodic over 180 degrees, Figure 3 shows that steady state is achieved in about four cycles for the three operating conditions tested in this study. A base grid of 6 mm is used for simulating the base cases. Additionally, for case 26, three more grids of 8 mm, 5 mm, and 4 mm have been used to show grid

convergence. The indicated power calculations are done by integrating the Pressure-Volume curve over the entire cycle.

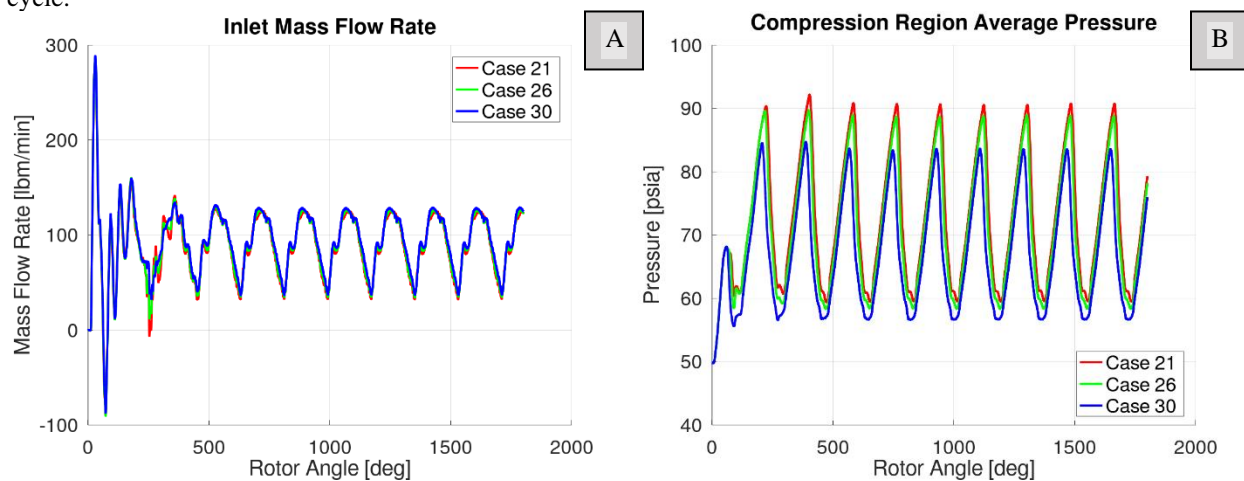


Figure 3: (A) shows Inlet mass flow rate as a function of time, (B) shows average pressure in the compressor region as a function of time

4.1 Comparison with measurements and grid comparison

Figure 5 shows the pressure field and Figure 6 shows the velocity field at different times for case 26. The compression phase of the cycle begins when the vane tip passes beyond the suction manifold when the volume of the chamber is maximum. It is then compressed as the rotor and vane move towards the discharge manifold. The pressure increases until it is high enough for the valves to start opening and the gas to start moving into the discharge manifold via the valves. Figure 4 shows the steady-state valve lift for all the valves over 180 degrees. The valve posts allow a maximum displacement of 5 mm. The valves in group 1 have one peak, in group 2 have two peaks and valve 3 has 3 peaks. The first peak for all three groups occurs when the vane is passing over the valves in group one. The pressure starts dropping once the vane moves past the valve in group 1, and the valves start closing. The pressure starts rising once the vane moves past the valves in group 1 and the valves in groups 2 and 3 start opening again, eventually leading to the second peak, similar mechanism exists for the third of valve 3. The entire compression cycle for case 21 is shown in Figure 5. The results match the experimental data very well. The simulation predicts lower pressures towards the end of the compression cycle. This is largely explained by the assumption of constant discharge pressure at the outflow, while the experiments have fluctuations in the discharge pressure.

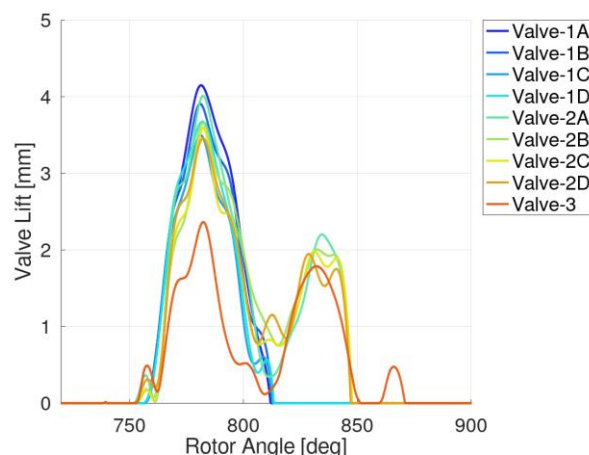


Figure 4: Valve lift as a function of time for case 26

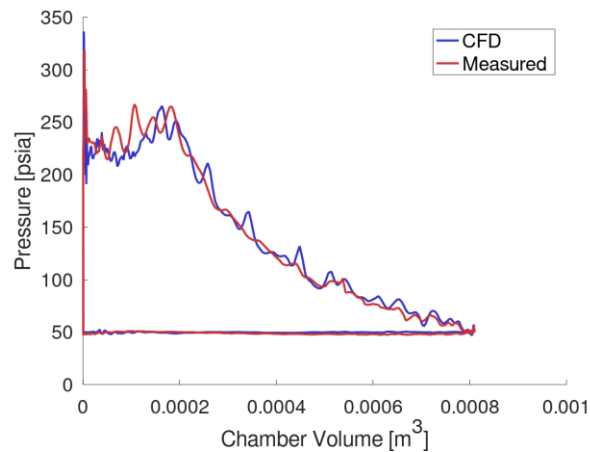


Figure 5: Steady state Pressure-Volume curve for case 21

The simulation yields similar results for the other two cases as well. Figure 8A shows that the mass flow rate predicted by the simulation is very close to the measure data, maximum deviation is observed for case 26 which was around 1.54%. The power comparison also shows a similar trend as observed in Figure 8B. The indicated power between the simulation and experiment is fairly similar to each other with a maximum error of around 6% for case 30. Table 2 shows the values of flow rates and power calculated along with percentage errors when compared to measured data.

Case	Flow rate [lb./min]	Error [%]	Indicated Power [kW]	Error [%]
Case 21	89.56	1.15	29.54	1.23%
Case 26	91.07	1.54	26.50	3.42%
Case 30	93.96	0.75	20.63	6.23%

Table 2: Cycle averaged flow rates and indicated power for the three cases

For CFD simulations, it is essential to show the choice of grid size used for the study is fine enough to make the numerical error be less than the modeling error while maintaining a relatively low computational cost. A grid convergence study was performed for case 26 for four different grid sizes. Table 3 shows the mass flow rates and indicated power for various grid sizes. The flow rate varies by 0.11% and indicated power varies by -1.45% when the grid changes from 6mm to 4mm. The average cell counts and run time per cycle are also presented in Table 3. The 6mm grid size case shows grid convergence with a reasonable run time for practical engineering applications.

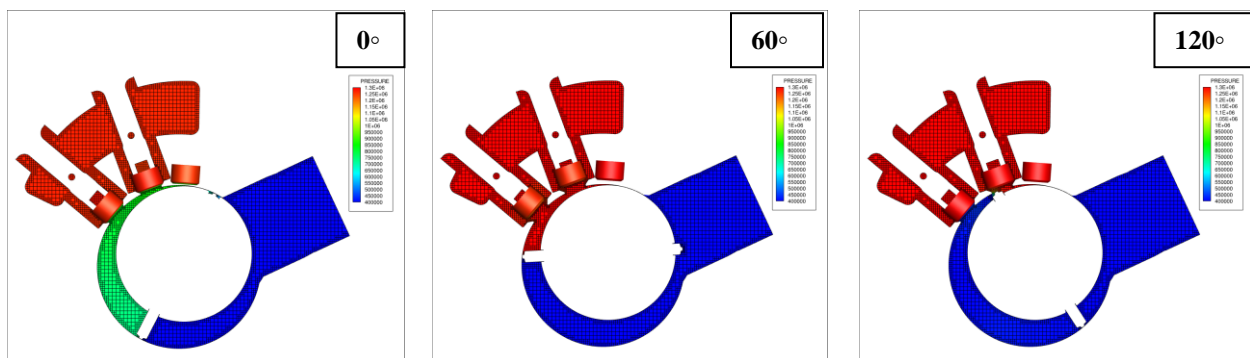


Figure 6: Cut plane along the compression chamber and valve 1A, 2A and 3 colored by pressure with grid

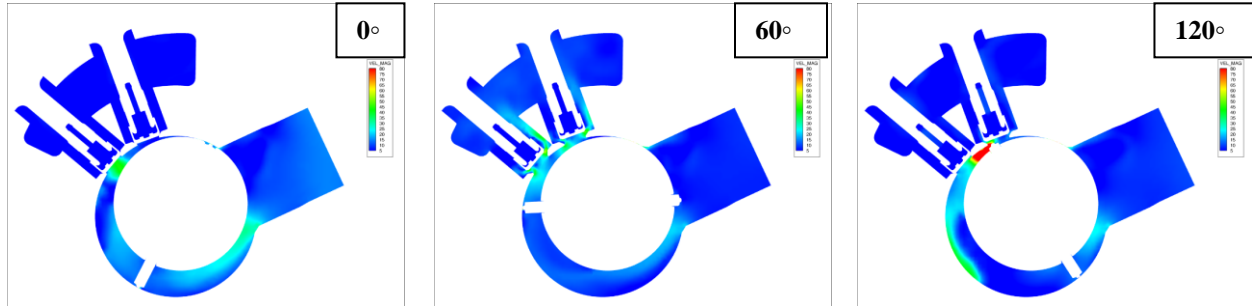


Figure 7: Cut plane along the compression chamber colored by velocity magnitude for case 26

Base grid size [mm]	Cell count [million cells]	Time/180 deg [hrs.]	Mass flow rate [lb./min]	Power [kW]
8.0	0.38	6	89.85	23.12
6.0	0.75	13	91.04	23.06
5.0	1.15	21	90.64	22.92
4.0	1.93	38	91.26	22.80

Table 3: Run time and cell count data for the four grids

5. CONCLUSIONS

This work presents a first validation study using cut-cell based method for simulating a rotary spool compressor. The method displays a lot of advantages for simulating this compressor with complicated geometry and multiple moving parts. Additional models are applied to model the slip flow through the small gaps, allowing the usage of coarse grids and saving computational costs. The orthogonal cells used to mesh the fluid domain ensure low numerical diffusion, high numerical accuracy, and stability. Additionally, AMR ensures more cells are allocated in regions with high gradients for velocity and pressure, which focuses the computational resources in the relevant regions at any given part of the cycle. The results show a good match with the experimental data. Further grid sensitivity analysis was performed, and a base grid of 6 mm was chosen as a compromise between accuracy and run time. The run time achieved for this was low enough to be used for engineering purposes, while further optimization can be made to reduce the computational cost and run time.

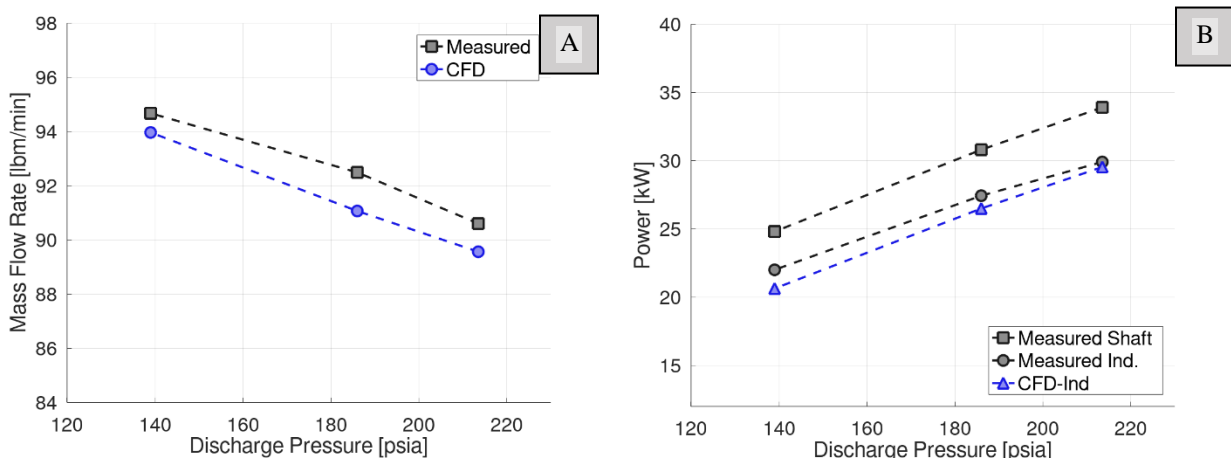


Figure 8: (A) shows the mass flow rates as a function of discharge pressure comparing measured data (black squares) with CFD data (blue circles) (B) Shows power as a function of discharge pressure comparing shaft power (black squares), measured indicated power (black circles) and indicated power from the CFD data (blue triangles)

NOMENCLATURE

F	Force	(N)
m	Mass	(kg)
\ddot{x}	Acceleration	(m ² /s)
Subscript		
total	Total	

REFERENCES

- Bell, I. H., Wronski, J., Quoilin, S., Lemort, V. (2014). Pure and Pseudo-pure Fluid Thermophysical Property Evaluation and the Open-Source Thermophysical Property Library CoolProp. *Industrial & Engineering Chemistry Research*, 53 (6), 2498-2508.
- Bradshaw, C., Kemp, G., Orosz, J., Groll, E., 2012. A Comprehensive Model of a Novel Rotating Spool Compressor. In: *Proceedings of the International Compressor Engineering Conference*. Purdue University, West Lafayette, IN USA. No. 1142.
- Bradshaw, C., Kemp, G., Orosz, J., Groll, E., 2016. Design Methodology Improvements of a Rotating Spool Compressor using a Comprehensive Model. In: *Proceedings of the International Compressor Engineering Conference*. Purdue University, West Lafayette, IN USA. No. 1376.
- Issa, R. I. (1985). Solution of the Implicitly Discretised Fluid Flow Equations by Operator-Splitting. *Journal of Computational Physics*, 62.
- Kemp, G., Garrett, N., Groll, E., 2008. Novel Rotary Spool Compressor Design and Preliminary Prototype Performance. In: *Proceedings of the International Compressor Engineering Conference*. Purdue University, West Lafayette, IN USA. No. 1328.
- Pomraning, E., Richards, K., and Senecal, P. (2014). Modeling Turbulent Combustion Using a RANS Model, Detailed Chemistry, and Adaptive Mesh Refinement. *SAE Technical Paper*, #2014-01-1116.
- Rhie, C. M. & Chow, W. L. (1983). Numerical Study of the Turbulent Flow Past an Airfoil with Trailing Edge Separation. *AIAA J.*, 21, (pp. 1525-1532).
- Pham, H., Brandt, T., Rowinski, D., 2018. Modeling a Scroll Compressor Using a Cartesian Cut-Cell Based CFD Methodology with Automatic Adaptive Meshing. In: *Proceedings of the International Compressor Engineering Conference*. Purdue University, West Lafayette, IN USA. No. 1252.
- Rowinski, D., Li, Y., Bansal, K. 2018. Investigations of Automatic Meshing in Modeling a Dry Twin Screw Compressor. In: *Proceedings of the International Compressor Engineering Conference*. Purdue University, West Lafayette, IN USA. No. 1528
- Rowinski, D., Nikolov, A., Brummer, A. 2018. Modeling a dry running twin-screw expander using a coupled thermal-fluid solver with automatic mesh generation. *International Conference on Screw Machines*, TU-Dortmund.
- Rowinski, D., Sadique, J., Oliveira, S., Marcelo, R., 2018. Modeling a Reciprocating Compressor Using a Two-Way Coupled Fluid and Solid Solver with Automatic Grid Generation and Adaptive Mesh Refinement. In: *Proceedings of the International Compressor Engineering Conference*. Purdue University, West Lafayette, IN USA. No. 1587.
- Senecal, P. K., Pomraning, E., Richards, K. J., Briggs, T. E., Choi, C. Y., McDavid, R. M., Patterson, M. A., Hou, S., & Shethaji, T. (2007). A New Parallel Cut-Cell Cartesian CFD Code for Rapid Grid Generation Applied to In-Cylinder Diesel Engine Simulations. *SAE Technical Paper*, #2007-01-0159.

Tillner-Roth, R. & Baehr, H.D. (1994). An international standard formulation of the thermodynamic properties of 1,1,1,2-tetrafluoroethane (HFC-134a) covering temperatures from 170 K to 455 K at pressures up to 70 MPa. J. Phys. Chem. Ref. Data, 23, 5, 657-729

Yakhot, V. & Orszag, S. A. (1986). Renormalization Group Analysis of Turbulence. I. Basic Theory. J. Sci. Comput., 1, 3.

Yarborough, S., Bradshaw, C., Kemp, G., Orosz, J., 2021. Empirical Indicated Loss Analysis of a Semi-hermetic Light-Commercial Spool Compressor. In: Proceedings of the International Compressor Engineering Conference. Purdue University, West Lafayette, IN USA. No. 1236.

Zhang, Z., Rowinski, D. Bansal, K. 2019. Analysis of a rolling piston compressor through a coupled fluid and solid solver with automated mesh generation. In: Proceedings of. 9th International Conference on Compressors and Refrigeration (ICCR)